Near# and Mid#Infrared Photometry of High# Redshift 3CR Sources

The Astrophysical Journal, 688:122–127, 2008 November 20

NEAR- AND MID-INFRARED PHOTOMETRY OF HIGH-REDSHIFT 3CR SOURCES

Martin Haas,[1] S. P. Willner,[2] Frank Heymann,[1,3] M. L. N. Ashby,[2] G. G. Fazio,[2]
Belinda J. Wilkes,[2] Rolf Chini,[1] and Ralf Siebenmorgen[3]
Received 2008 May 30; accepted 2008 July 18

ABSTRACT

Using the *Spitzer Space Telescope*, we have obtained 3.6–24 μm photometry of 38 radio galaxies and 24 quasars from the 3CR (Third Cambridge Revised Catalog of Radio Sources) at redshift $1 < z < 2.5$. This 178 MHz selected sample is unbiased with respect to orientation and therefore suited to study orientation-dependent effects in the most powerful active galactic nuclei (AGNs). Quasar and radio galaxy subsamples matched in isotropic radio luminosity are compared. The quasars all have similar spectral energy distributions (SEDs), nearly constant in νF_ν through the rest 1.6–10 μm range, consistent with a centrally heated dust distribution that outshines the host galaxy contribution. The radio galaxy SEDs show larger dispersion, but the mean radio galaxy SED declines from rest 1.6 to 3 μm and then rises from 3 to 8 μm. The radio galaxies are on average a factor 3–10 less luminous in this spectral range than the quasars. These characteristics are consistent with composite emission from a heavily reddened AGN plus starlight from the host galaxy. The mid-infrared colors and radio to mid-infrared spectral slopes of individual galaxies are also consistent with this picture. Individual galaxies show different amounts of extinction and host galaxy starlight, consistent with the orientation-dependent unified scheme.

Subject headings: galaxies: active — infrared: galaxies — quasars: general

Online material: color figures

1. INTRODUCTION

When exploring the general evolution of galaxy populations across cosmic times, a particular challenge is to distinguish between black hole and star-forming activity. Star formation and obscuring dust go hand in hand, and black hole–driven active galactic nuclei (AGNs) are also surrounded by dust mainly distributed in a disk/torus-like geometry (Antonucci 1993). There is evidence that AGNs mainly power the near- and mid-IR emission (NIR, $\sim$2 μm; MIR, $\sim$10 μm) from hot nuclear dust, while starbursts contribute mainly to the far-infrared (FIR, $\sim$60 μm) luminosity (e.g., Rowan-Robinson 1995; Vernet et al. 2001; Schweitzer et al. 2006). Using the MIR/FIR luminosity ratio as an indicator for the relative AGN and starburst contributions, numerous studies have found an increase of AGN/starburst activity with total luminosity and redshift, but the validity of this trend is still under discussion because of selection effects on the various samples. More seriously, an unfavorable AGN orientation could cause MIR obscuration (e.g., Pier & Krolik 1993), leading to a fundamental observational degeneracy: a low MIR/FIR luminosity ratio can be due to either a high star-forming contribution or to an AGN in which the hot dust is obscured. The spectral energy distribution (SED) of an obscured AGN may thus mimic that of a starburst-powered source. While this degeneracy has now been widely examined at low/intermediate luminosity and redshift ($z < 1$), it has still to be explored for the most luminous sources at high redshift ($z > 1$). In order to assess galaxy and AGN evolution in the universe, we therefore need to understand this AGN/starburst degeneracy for a population of luminous high-redshift sources. A crucial step toward this is to study the orientation dependence of the NIR and MIR emission of high-redshift AGNs.

Orientation-dependent effects can only be tested and quantified with AGN samples having type 1 (unobscured) and type 2 (obscured) subsamples matched in isotropic emission. The clean AGN tracers—optical, [O III] λ5007, NIR, and X-ray ($\lesssim$10 keV)—all fail to fulfill this requirement. The [O II] λ3727 emission, while isotropic (Hes et al. 1993), is probably dominated by extended starbursts and shocks (Best et al. 2000) rather than by the AGN. Therefore, the only feasible way is low-frequency (meter-wavelength) radio selection because the integrated emission from the radio lobes is optically thin and essentially isotropic. This makes radio-loud AGNs particularly attractive for studying orientation-dependent properties at other wavelengths and, after sorting out the influence of radio jets/lobes on the emission, for generalizing conclusions about orientation-dependent effects on the much larger population of radio-quiet AGNs.

The brightest low-frequency-selected AGN sample is the 3CR compilation (Spinrad et al. 1985). The powerful double-lobed radio galaxies (henceforth simply called radio galaxies) are supposed to be misaligned quasars (Barthel 1989). Based on *IRAS* co-added scans and a few individual detections, Heckman et al. (1992, 1994) already noted an average MIR/FIR difference between 3CR quasars and radio galaxies. More comprehensive MIR and FIR spectrophotometry from *ISO* is in hand (as compiled by Siebenmorgen et al. [2004] and by Haas et al. [2004]) as well as from *Spitzer* (e.g., Shi et al. 2005; Haas et al. 2005; Ogle et al. 2006; Cleary et al. 2007), providing a basis to study the $z < 1$ 3CR objects. These sources are, however, a factor of 5 less radio luminous on average than the most powerful radio sources seen at higher redshift, and the lower indicated accretion power may reflect different source physics. The higher luminosity population can be sampled by the 3CR sources at $1 < z < 2.5$, which have radio luminosities similar to those of the most powerful radio sources at even higher redshift ($2.5 < z < 6$). However, with the exception of a few targets (Siebenmorgen

[1] Astronomisches Institut, Ruhr-Universität Bochum, Universitätsstraße 150, 44801 Bochum, Germany; haas@astro.rub.de.
[2] Harvard-Smithsonian Center for Astrophysics, 60 Garden Street, Cambridge, MA 02138.
[3] European Southern Observatory, Karl-Schwarzschildstrasse 2, 85748 Garching, Germany.

et al. 2004; Seymour et al. 2007), the high-z 3CR sample has not been well observed in the rest-frame NIR and MIR.

This paper is based on *Spitzer* observations of 62 of the 64 high-z 3CR sources. It focuses on the hot nuclear dust emission and its obscuration in the most luminous type 2 AGNs. We use a ΛCDM cosmology with $H_0 = 71$ km s^{-1} Mpc^{-1}, $\Omega_m = 0.27$, and $\Omega_\Lambda = 0.73$.

2. OBSERVATIONS AND DATA

With the *Spitzer Space Telescope* (Werner et al. 2004), we are observing the entire sample of 64 high-z 3CR sources using the instruments IRAC (3.6–8.0 μm, Fazio et al. 2004), the IRS blue peak-up array (16 μm, Houck et al. 2004), and MIPS (24 μm, Rieke et al. 2004). Most observations are performed in our guaranteed time program (PID 40072; PI: G. Fazio) with on-source exposure times 4×30 s (each IRAC band), 4×14 s (IRS), and 10×10 s (MIPS). A few sources have been observed in other programs, and we use the published photometry if available (e.g., PID 3329; PI: D. Stern; Seymour et al. 2007).

For IRAC, we used the basic calibrated data products (BCD, ver. S16) and co-added them to 0.869″ pixels using the latest version of IRACProc (Schuster et al. 2006). This optimally handles the slightly undersampled IRAC point-spread function (PSF) in order to ensure accurate point-source photometry. For IRS, we used the post-BCD pipeline product, version S16. For MIPS, we used custom routines to modify the version S17 BCD files to remove instrumental artifacts (e.g., residual images) before shifting and co-adding to create the final mosaics. All sources are well seen on the images in all filters. The sources were extracted and matched using the SExtractor tool (Bertin & Arnouts 1996). We used sufficiently large apertures so that aperture corrections are small (<5%). The photometric errors are typically smaller than 10% but increase for faint sources; exceptions are 3C 225A and 3C 294, where nearby bright stars make the photometry uncertain in the shorter IRAC bands.

As of 2008 April, 24 quasars and 38 radio galaxies have been observed, covering the complete high-z 3CR sample with the exception of the quasar 3C 245 and the radio galaxy 3C 325. All 62 sources have IRAC measurements and are observed in at least one of the 16 and 24 μm bands (54 sources at 16 μm and 60 sources at 24 μm).

For the analysis it is desirable to compare rest-frame SEDs with the same wavelength sampling. Depending on the redshift of our sources ($1 < z < 2.5$) the observations sample different rest wavelengths between 1.6 and 10 μm. Before resampling and interpolating the SEDs, we checked that spectral features do not affect the interpolation. In principle, prominent spectral features in this wavelength range could be polycyclic aromatic hydrocarbon (PAH) emission bands around 7.7 μm and the 9.7 μm silicate absorption feature. IRS spectra of several low-z and even a few high-z FR II radio sources are available. PAH features are weak and usually undetected, and the continua are generally smooth. Strong silicate absorption is, however, present in some objects (Haas et al. 2005; Ogle et al. 2006; Cleary et al. 2007; Seymour et al. 2008). Our broadband SEDs therefore represent the smooth continua for $\lambda \lesssim 8$ μm but are uncertain at rest wavelengths near 10 μm. In practice, the deredshifted SEDs were interpolated in log-log space at 12 wavelengths between rest 1.6 and 10 μm to produce the figures shown.

The quasar and radio galaxy samples match reasonably well in redshift and rest-frame 178 MHz flux density. Rest-frame 178 MHz radio flux densities were derived from data listed in the NASA Extragalactic Database (NED). The quasars have mean redshift $\langle z \rangle = 1.44 \pm 0.31$ and mean flux density $\langle S_{178} \rangle = 27.8 \pm 15.1$ Jy, while the values for the radio galaxies are $\langle z \rangle = 1.42 \pm 0.31$, $\langle S_{178} \rangle = 22.2 \pm 6.2$ Jy. Thus, over the whole sample, quasars are about 30% more luminous than radio galaxies, as shown in Figure 1. In order to improve the luminosity match, we have excluded the sources at the low and high ends of the distribution, $L_{178} < 1.8 \times 10^{44}$ and $L_{178} > 1.5 \times 10^{45}$ ergs s^{-1}, respectively.

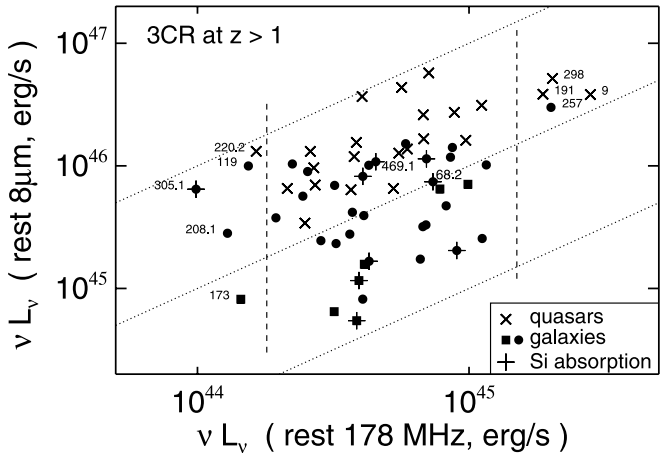

FIG. 1.—Infrared vs. radio luminosity of the 3CR sample at $z > 1$ prior to normalization. Crosses denote quasars; circles and squares denote radio galaxies. Superposed plus signs indicate radio galaxies that show evidence of silicate absorption (§ 3.1). The vertical dashed lines mark the range of our luminosity-matched quasar and radio galaxy subsamples. The dotted lines indicate $L_{8\,\mu m}/L_{178\,MHz}$ ratios of 1, 10, and 100. The radio galaxies are grouped into several SED classes in Fig. 3 and § 3.1. The color coding and symbols are: *green circle* (A), *red circle* (B), *red square* (C), *blue square* (D), *blue circle* (E). The two low-excitation radio galaxies 3C 68.1 and 3C 469.1 are labeled with their 3C numbers, as are sources outside the luminosity range of our analysis. [*See the electronic edition of the Journal for a color version of this figure*.]

We have also excluded the quasar 3C 418 because of its flat radio spectrum (low-frequency spectral index $\alpha_{178} \approx 0$), while all other sources have steep radio spectra ($-1.1 \lesssim \alpha_{178} \lesssim -0.6$). The resulting mean radio luminosities of the sample galaxies are $\langle L_{178} \rangle = (5.35 \pm 2.53) \times 10^{44}$ ergs s^{-1} for quasars and $(5.55 \pm 2.34) \times 10^{44}$ for radio galaxies.

While the quasar and radio galaxy distributions match very well in L_{178}, a proper analysis of orientation-dependent effects requires also that the individual SEDs are normalized by the radio luminosity, which serves as a tracer for the intrinsic AGN strength. Therefore, we have normalized each SED to the sample mean 178 MHz luminosity; after normalization each object has $L_{178} = 5.4 \times 10^{44}$ ergs s^{-1}. Because of the good L_{178} match of the samples, it turned out that the net effect of this normalization on the results is small.

3. RESULTS AND DISCUSSION

3.1. *Radio Galaxies as Obscured Quasars*

The NIR–MIR SEDs of quasars are all very similar in shape, as shown in Figure 2. The SEDs can be described by a single power law $L_\nu \propto \nu^{-1}$, consistent with previous results for lower redshift objects (e.g., Elvis et al. 1994). The dispersion of the SEDs is essentially caused by differing ratios of MIR to radio luminosity. Some quasars exhibit small (10%–20%) bumps around 5 μm explainable by distinct hot dust components.[4] The

[4] Despite the similarity of the infrared SEDs, the quasar population is not homogeneous at optical wavelengths: there are quasars like 3C 186, with blue optical SED, and 3C 68.1, with red optical SED, as listed in NED. In the orientation-based unified scheme, 3C 68.1 could be borderline so that the broad lines are detected, but most of the UV-optical continuum is absorbed.

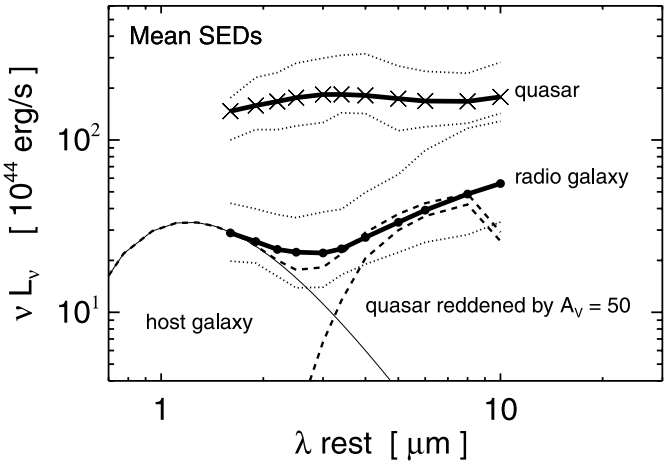

FIG. 2.—Rest-frame quasar and radio galaxy SEDs normalized by rest 178 MHz luminosity ($\langle L_{178} \rangle = 5.4 \times 10^{44}$ ergs s^{-1}). Symbols connected with thick blue and red lines show the mean SEDs for quasars and radio galaxies, respectively. The thin dotted blue and red lines indicate the dispersion (upper and lower quartiles) around the mean SEDs; the mean ratios of upper/lower quartiles are 2.3 (quasars) and 3.4 (radio galaxies). The radio galaxy SED can be explained by the sum (*black dashed line*) of a reddened quasar (*blue dashed line*) and starlight from the host galaxy (*thin black solid line*). The dashed lines have been shifted slightly to make them visible in the plot. The difference between radio galaxies and reddened quasars at 10 μm may be due to the silicate absorption feature, which may escape detection in our broadband photometry. [*See the electronic edition of the Journal for a color version of this figure.*]

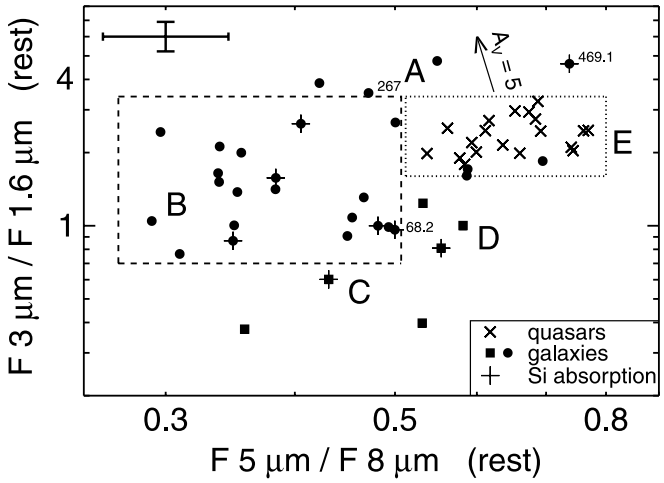

FIG. 3.—NIR/MIR color-color diagram. The radio galaxies are grouped into five classes, labeled A–E as explained in § 3.1. Symbol color coding is the same as in Fig. 1. Radio galaxies with a photometric signature for silicate absorption are additionally marked with an underlying plus sign. The two sources 3C 267 and 3C 469.1 with spectroscopically detected silicate absorption are labeled, as are the two low-excitation radio galaxies 3C 68.1 and 3C 469.1. The error bar in the upper left corner represents a color rms of 15%. The A_V arrow indicates screen extinction with the reddening law given in § 3.1. [*See the electronic edition of the Journal for a color version of this figure.*]

power-law shape of the quasar SED can naturally be explained by the superposition of centrally heated dust components with a radial temperature gradient (1500 K $> T >$ 300 K), as has been found also in lower luminosity type 1 AGNs (e.g., Ward et al. 1987; Barvainis 1987; see also Rowan-Robinson 1980). Any contribution of the quasar host galaxies to the NIR–MIR SEDs appears to be outshone (factor $\gtrsim$5–10) by the AGN dust emission.

In contrast to quasars, radio galaxies display a diversity of SED shapes leading to a 50% larger dispersion around their mean SED (Fig. 2). Despite the dispersion, nearly all radio galaxy SEDs show a decline from rest 1.6 μm to 3 μm and a rise from 3 μm to 8 μm ($L_\nu \propto \nu^{-1.9}$). In addition, the average radio galaxy SED is fainter by a factor of 3 at 8 μm and a factor of 8 at 2 μm relative to the quasar SED. Unlike the quasars, hot ($T > 750$ K) dust emission is not seen in the radio galaxy SEDs. Its absence can be explained by absorption (screen $A_V \approx 50$)[5] of the central dust emission. The short-wavelength ($\lambda < 3$ μm) component can then be explained by emission from stars in the host galaxy. Extrapolation of the mean 3–8 μm SED slopes toward longer wavelengths suggests that the radio galaxy and quasar SEDs meet each other at about 25–40 μm, and beyond these wavelengths extinction may be no longer relevant.

As noted above, the quasar NIR–MIR SED shapes are extremely homogeneous. This is reflected in the narrow range of the quasars' NIR and MIR colors. The color-color diagram shown in Figure 3 illustrates the differing SED types. In this diagram, quasars populate a distinct locus (E), while radio galaxies show wider dispersion as mentioned above. According to their location in the color-color diagram, we have grouped the radio galaxies into five classes described below. Their SED shapes are illustrated in Figure 4.

A. Four sources at the high end of the 3 μm to 1.6 μm ratio (above the dotted and dashed boxes in Fig. 3): basically, they have quasar-like SEDs, but the hottest dust emission at about 1–2 μm appears to be absorbed (screen $A_V \approx 5$), leading to a redder 3 μm to 1.6 μm color compared to quasars.

B. The bulk of radio galaxies (20 sources) have declining 1–3 μm SEDs with a steep 3–8 μm rise. Their colors can be explained by a heavily reddened AGN plus an added component of starlight contributing at 1.6 μm. If this explanation is correct, the direction of the extinction vector A_V becomes

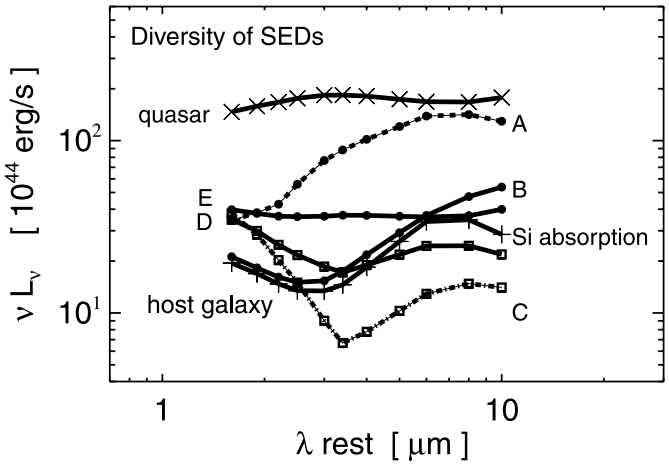

FIG. 4.—Mean SED of each radio galaxy class as identified in § 3.1. The SEDs have been normalized to the mean 178 MHz luminosity. The mean quasar SED is also shown for comparison. The dispersion around each SED (measured as mean ratio of upper/lower quartile) is 2.3 (quasars), 2.0 (A), 3.2 (B), 2.4 (C), 1.7 (D), 1.5 (E), and 4.8 (silicate absorption). [*See the electronic edition of the Journal for a color version of this figure.*]

[5] The reddening curve used is a compromise between the latest results for Milky Way reddening and earlier data (summarized by Indebetouw et al. 2005): $A_V/A_H/A_{3\,\mu m}/A_{5\,\mu m}/A_{8\,\mu m}/A_{10\,\mu m} = 1/0.184/0.070/0.037/0.028/0.040$.

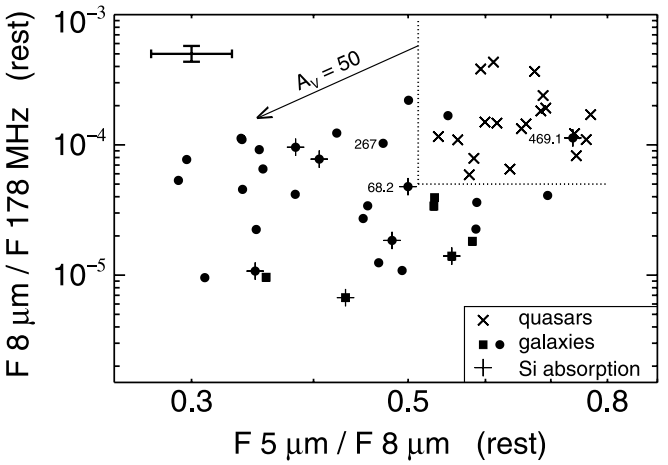

FIG. 5.— Infrared-radio color-color diagram. The dotted line marks the region occupied by quasars. The color coding and symbols of radio galaxies correspond to those in Figs. 1 and 3. The two sources 3C 267 and 3C 469.1 with spectroscopically detected silicate absorption are labeled, as well as the two low-excitation radio galaxies 3C 68.1 and 3C 469.1. The error bar in the upper left corner represents an rms of 15%. The A_V arrow indicates screen extinction with the reddening law given in § 3.1. [*See the electronic edition of the Journal for a color version of this figure*.]

meaningless because host galaxy starlight will not be affected by extinction near the nucleus. Instead, vertical position in the plot is determined by the relative contributions of starlight and AGN light, while horizontal position measures the amount of extinction (to the extent the underlying AGN SEDs are the same). As noted above, $A_V \sim 50$ mag is required to explain the colors.

C. Three sources at the low end of the 3 μm to 1.6 μm ratio (below the long dashed line in Fig. 3): their SEDs show a very strong host galaxy contribution at 1.6 μm, and starlight exceeds the dust luminosity even at wavelengths as long as 3.5 μm. In principle, class C is similar to class B but with stronger host galaxy contribution.

D. Three sources immediately below the dotted box in Figure 3: their SEDs can be explained by a slightly reddened AGN (similar to class A) plus an added component of starlight contributing significantly at 1.6–3 μm.

E. Three sources with quasar-like SED colors (inside the dotted box in Fig. 3): their SEDs overlap with the low-luminosity end of the quasar SEDs. In the orientation-based unified scheme, these sources could be borderline so that most of the dust torus is visible but the broad-line region and the UV-optical continuum are obscured.

While the rest 8–10 μm range is poorly sampled, eight galaxies show declines in this range that could be caused by silicate absorption. (The MIPS-24 filter, 50% transmission at 20.8–29.3 μm, requires $z \lesssim 1.8$ for the silicate feature to fall into its range.) One of these sources (3C 469.1, $z = 1.336$) has an IRS spectrum available. It shows a broad silicate absorption with optical depth $\tau_{9.7} \approx 0.55$ corresponding to $A_V \approx 10$, consistent with its position in Figure 3. This supports the view that the SED declines in the other radio galaxies are due to silicate absorption, too. The photometric silicate absorption sources show a wide range of colors (Fig. 3), but only one galaxy (3C 469.1) is on the blue (right) side, where low-extinction sources reside. The important conclusion is that the silicate feature requires considerable extinction to be present in at least some of the radio galaxies, and this is largely independent of the SED class.[6]

If radio galaxies are misaligned quasars, as proposed in the unified scheme, reddening of individual galaxies should be correlated with their extinction. Figure 5 shows that this is indeed the case. Quasars populate a distinct region of this diagram characterized by high MIR/radio and blue NIR–MIR colors. Most radio galaxies spread toward fainter MIR/radio and redder NIR/MIR. Under the reasonable assumption that the emission at 5–8 μm is not affected by the host galaxy, dereddening along the direction of the extinction vector can place each radio galaxy inside the region populated by quasars. Thus, individual radio galaxies can be explained as reddened quasars, consistent with the orientation-dependent unified scheme.

The typical amount of radio galaxy reddening, $A_V \approx 50$ for an obscuring screen (Fig. 5), corresponds to a hydrogen column density $N_{\rm H} \approx 9 \times 10^{22}$ cm^{-2} (for $A_V = 5.6 \times 10^{-22}$ mag cm^2; Seward 1999). This is close to but below the Compton-thick limit ($N_{\rm H} = 10^{24}$ cm^{-2}). Screen extinction is a simplification, and one may expect a more complex geometry. If emitting dust particles are spatially mixed with the absorbing ones, the amount of dust has to be higher for the same observed reddening, typically by a factor of 3–5.[7] Thus there could very well be enough gas present to render the AGN Compton-thick.

There is, unfortunately, no independent measurement of reddening for individual galaxies, nor is it certain that a Galactic reddening curve applies to AGNs. Thus it is still an open question whether after dereddening there will remain a difference in the 8 μm to 178 MHz ratio between radio galaxies and quasars. If such a difference remains, with quasars having a higher 8 μm to 178 MHz ratio than radio galaxies, then either our screen extinction premise is too simple or the MIR luminosity of quasars is enhanced by an additional—potentially nonthermal—contribution. Our *Chandra* X-ray observations of a subset of the sample will provide independent estimates of the extinction toward the nuclei (B. J. Wilkes et al. 2008, in preparation).

To summarize, while quasars exhibit a uniform SED shape that can be explained by a centrally heated dust distribution, radio galaxies show a diversity of SED shapes. In all cases, however, the radio galaxy SEDs are consistent with being intrinsically a quasar modified by absorption of the dust emission and addition of some amount of host galaxy starlight.

3.2. *Evolutionary Effects and Nonthermal Contributions*

Studying powerful 3CR sources at $z < 1$, Ogle et al. (2006) found evidence for a population of accretion-inefficient radio

[6] The photometric silicate absorption sources are 3C 68.2, 3C 222, 3C 249, 3C 250, 3C 266, 3C 305.1, 3C 324, and 3C 469.1. These galaxies lie in the redshift range $1.08 < z < 1.83$, suggesting that in this range the broad band 16 μm to 24 μm filter combination is able to register silicate absorption, if strong enough. For comparison, this redshift range contains 20 more radio galaxies with 16 and 24 μm photometry available but without silicate absorption signatures in their broadband SEDs. Four of these sources (3C 13, 3C 266, 3C 267, 3C 356) have IRS spectra available, but significant silicate absorption is detected only in one of them (3C 267, $z = 1.14$, $\tau_{9.7} \approx 0.2$). At low redshift, the detection of silicate absorption appears not to be directly correlated with other absorption signatures, perhaps because of complex geometry and/or varying silicate dust abundance (e.g., Haas et al. 2005; Ogle et al. 2006; Cleary et al. 2007). A detailed analysis of the high-z 3CR spectra and the photometric detectability of silicate features will be presented elsewhere (C. Leipski et al. 2008, in preparation).

[7] The transmission factors are $\exp(-\tau_\lambda)$ and $[1 - \exp(-\tau_\lambda)]/\tau_\lambda$ for the screen and the mixed case, respectively, with $\tau_\lambda = 0.916 A_\lambda$ (Disney et al. 1989).

galaxies, in which the jet/lobe may be powered by extraction of rotational black hole energy. These sources, mainly optically classified low-excitation radio galaxies (LERGs), have a 15 μm luminosity below 8×10^{43} ergs s^{-1} and a luminosity ratio $L_{15\,\mu\mathrm{m}}/L_{178\,\mathrm{MHz}} < 10$. In contrast, with the reasonable assumption that $L_{8\,\mu\mathrm{m}} \lesssim L_{15\,\mu\mathrm{m}}$, all our $z > 1$ sources have observed MIR luminosity $L_{8\,\mu\mathrm{m}} > 5 \times 10^{44}$ ergs s^{-1}, which is expected to be even higher after dereddening. Also, the two LERGs (3C 68.2, 3C 469.1) in our sample show a high luminosity ratio $L_{8\,\mu\mathrm{m}}/L_{178\,\mathrm{MHz}} > 10$, comparable to that of quasars (Fig. 1). From this, our data do not support the existence of an accretion-inefficient population among the powerful 3CR sources at $z > 1$. A possible explanation for the deficit of optical high-excitation line luminosity (for instance, [O III] λ5007) in our two LERGs may be extinction of the narrow-line region. On the other hand, some of our radio galaxies with very strong host contribution (plotted as squares in Fig. 5) are expected after dereddening to lie at the low end of the $L_{8\,\mu\mathrm{m}}/L_{178\,\mathrm{MHz}}$ distribution. Hence, compared with the strength of both the host and the radio lobes, these galaxies are relatively weak in the MIR and may represent a population at the beginning of a different evolutionary state.

Some authors have attributed the excess emission of quasars compared to radio galaxies to nonthermal emission from synchrotron jets. For example, Cleary et al. (2007) fitted the SEDs and spectra of 3CR sources at $0.5 < z < 1$ with a combination of a spherically symmetric dust model and a jet+lobe synchrotron component. They attributed half of the factor of 4 excess in the 15 μm luminosities of steep-spectrum quasars relative to radio galaxies to a nonthermal component. If such a nonthermal component were present in our 3CR sources at $z > 1$, it would show up in Figure 5 as an offset by about a factor of 2 between dereddened radio galaxies and quasars. This conclusion is, however, dependent on both the reddening law and on the radiative transfer and thus the geometry of the emitting region. In order to draw definite conclusions about any MIR luminosity excess, detailed radiative transfer modeling is required (F. Heymann et al. 2008, in preparation). Spherically symmetric models are wholly inadequate for this purpose. In an inclined disklike system, some fraction of the MIR emission is likely to have very little obscuration while the bulk of the MIR emission is heavily obscured, and no spherical model can properly account for this geometry. All we can say at the moment is that our data appear consistent with a simple thermal interpretation and show no evidence for a nonthermal component.

4. CONCLUSIONS

The 3CR sample at $1 < z < 2.5$ represents the most luminous steep-spectrum quasars (type 1 AGNs) and powerful double-lobed radio galaxies (type 2 AGNs). This sample is nearly unbiased by orientation. We have defined subsamples of 19 quasars and 33 radio galaxies matched in isotropic rest 178 MHz luminosity and have obtained *Spitzer* 3.6–24 μm photometry. The main results are:

1. Quasars all have similar energy distributions in the rest-frame 1.6–10 μm range, and their ratio of MIR to radio luminosity is also nearly constant. This is consistent with results seen previously in lower redshift samples.
2. The rest-frame 1.6–10 μm SEDs of radio galaxies can be explained as reddened quasars, consistent with orientation-dependent unification. Various amounts of extinction of the AGN emission combined with addition of host galaxy starlight can explain the diversity of radio galaxy SEDs.
3. If the extinction is sufficiently large, there is no need to invoke a beamed synchrotron contribution to explain the MIR luminosity difference between quasars and radio galaxies. The actual amount of extinction has to be derived from additional observations.
4. The above results hold also for splitting our sample in redshift and luminosity; within our sample we do not find any trends with redshift or luminosity.
5. At rest-frame 8 μm, quasars are 3 times more luminous than radio galaxies. If this difference applies also to high-redshift, radio-quiet AGNs, then MIR (24 μm) surveys are strongly biased in favor of type 1 and against type 2 AGNs. This will make it very difficult to resolve the AGN/starburst degeneracy with only broadband SEDs, and spectral line diagnosis will be required.

While our near-mid-IR SEDs provide a fundamental set of high-luminosity AGN templates, we expect to derive more stringent conclusions from proper two-dimensional radiative transfer modeling in combination with *Spitzer* MIR spectra, *Chandra* X-ray observations, and *Herschel* far-IR/submillimeter data.

This work is based on observations made with the *Spitzer Space Telescope*, which is operated by the Jet Propulsion Laboratory, California Institute of Technology, under a contract with NASA. Support for this work was provided by NASA through an award issued by JPL/Caltech. This research has made use of the NASA/IPAC Extragalactic Database (NED), which is operated by the Jet Propulsion Laboratory, California Institute of Technology, under contract with the National Aeronautics and Space Administration. M. H. is supported by the Nordrhein-Westfälische Akademie der Wissenschaften.

Facilities: Spitzer

REFERENCES

Antonucci, R. R. J. 1993, ARA&A, 31, 473
Barthel, P. 1989, ApJ, 336, 606
Barvainis, R. 1987, ApJ, 320, 537
Bertin, E., & Arnouts, S. 1996, A&AS, 117, 393
Best, P. N., Röttgering, H. J. A., & Longair, M. S. 2000, MNRAS, 311, 23
Cleary, K., et al. 2007, ApJ, 660, 117
Disney, M., Davies, J., & Phillipps, S. 1989, MNRAS, 239, 939
Elvis, M., et al. 1994, ApJS, 95, 1
Fazio, G. G., et al. 2004, ApJS, 154, 10
Haas, M., et al. 2004, A&A, 424, 531
———. 2005, A&A, 442, L39
Heckman, T. M., Chambers, K. C., & Postman, M. 1992, ApJ, 391, 39
Heckman, T. M., O'Dea, C. P., Baum, S. A., & Laurikainen, E. 1994, ApJ, 428, 65
Hes, R., Barthel, P. D., & Fosbury, R. A. E. 1993, Nature, 362, 326
Houck, J. R., et al. 2004, ApJS, 154, 18
Indebetouw, R., et al. 2005, ApJ, 619, 931
Ogle, P., Whysong, D., & Antonucci, R. R. J. 2006, ApJ, 647, 161
Pier, E. A., & Krolik, J. H. 1993, ApJ, 418, 673
Rieke, G. H., et al. 2004, ApJS, 154, 25
Rowan-Robinson, M. 1980, ApJS, 44, 403
———. 1995, MNRAS, 272, 737
Seward, F. D. 1999, in Allen's Astrophysical Quantities, ed. A. N. Cox (Berlin: Springer), 183

Schuster, M. T., Marengo, M., & Patten, B. M. 2006, Proc. SPIE, 6270, 627020
Schweitzer, M., et al. 2006, ApJ, 649, 79
Seymour, N., et al. 2007, ApJS, 171, 353
———. 2008, ApJ, 681, L1
Shi, Y., et al. 2005, ApJ, 629, 88
Siebenmorgen, R., Freudling, W., Krügel, E., & Haas, M. 2004, A&A, 421, 129
Spinrad, H., Marr, J., Aguilar, L., & Djorgovski, S. 1985, PASP, 97, 932
Vernet, J., Fosbury, R. A. E., Villar-Martín, M., Cohen, M. H., Cimatti, A., di Serego Alighieri, S., & Goodrich, R. W. 2001, A&A, 366, 7
Ward, M., et al. 1987, ApJ, 315, 74
Werner, M. W., et al. 2004, ApJS, 154, 1